A three-dimensional level set method for droplet sorting using a non-uniform electric field

Naz, N. and Sui, Y.

This is the author accepted version of the article published as N. Naz, Y. Sui; A three-dimensional level set method for droplet sorting using a non-uniform electric field. Physics of Fluids 1 August 2023; 35 (8): 082103. https://doi.org/10.1063/5.0160683

Submitted to Physics of Fluids

A three-dimensional level set method for droplet sorting using a non-uniform electric field

N. Naz[1, a)] and Y.Sui[2, b)]
[1)]*School of Engineering, Technology and Design, Canterbury Christ Church University, Canterbury, Kent, CT1 1QU, UK*
[2)]*School of Engineering and Materials Science, Queen Mary University of London, London E1 4NS.*

(Dated: 14 July 2023)

In this research, we have developed a computational method for droplet sorting using a non-uniform electric field. The method is based on a three-dimensional level-set method and the leaky-dielectric electrohydrodynamics (EHD) model. Level-set method is used for modelling the interface of the two-phase flow system. The electrostatic phenomenon is dealt with the leaky dielectric-leaky dielectric fluid system. At first, we validated our developed model for a classical flow case: a droplet subjected to a uniform electric field. The results obtained from the present computational method show good agreement with the existing results from the literature. After validation, we implemented the developed code in a practical application of droplet sorting using a non-uniform electric field (known as Dielectrophoresis- DEP) in a rectangular microchannel with an orthogonal side channel. We mainly focus on the sorting of the droplet without and with electric field effect as a function of different parameters of the problem. Depending on the intensity of the physical parameters, the droplet can flow into either the downstream main channel or it can sort into the orthogonal side branch. The sorting of a droplet is characterized by the critical branch ratio, q_c above which the droplet enters the side branch. The results and conclusions from the present thesis facilitate the understanding of the fundamental principles and mechanisms of electrohydrodynamics (EHD) based droplet sorting using dielectrophoresis in microfluidic channels. Therefore present results can have potential usefulness towards the design and development of droplet-based microfluidic devices.

I. INTRODUCTION

Electrohydrodynamics which is also known as EHD is an interdisciplinary branch of science which analyses the dynamics of electrically induced fluid flow through the coupling between electric and hydrodynamic forces. Application of electric field on a liquid droplet suspended in another medium leads to some fascinating fluid dynamics due to its ability to deformation, motion and break-up of the droplet. Several industries such as ink jet printing[1], electrospinning[2], atomization of fluids[3], biotechnology[4], material printing[5] involve the precise control of the size and morphology of the droplet when subjected to electric field. Another notable field of EHD is the sorting of droplet in microfluidic devices which are enormously used in biological research such as drug delivery[6,7], biological culture[8–10], cell sorting and separation for microfluidic systems[11] or industrial products such as cosmetics[12,13] and food additives[14].

In droplet based microfluidics, a number of external fields have been implemented for droplet manipulation such as electric[15,16], magnetic[17,18], accoustic[19,20] and pneumatic methods[21,22]. Among all of the these methods, sorting of droplet using non-uniform electric field also known as dielectrophoresis (DEP) is the most widely used sorting and separation techniques for microfluidics due to its high speed, efficiency, sensitivity and selectivity while maintaining a low running cost. DEP is a also label-free method and does not require any modification of sample during the sorting process. DEP is an effective way to trap[23–25] , separate and sort various types of cells such as breast cancer cells[26], red blood cells[27,28], viable yeast cells[29] and characterizing microorganisms[30], DNA[31], virus[32,33] and bacteria[34–36].

Thus understanding the fundamental principles and mechanism of EHD leading to the motion and deformation of the drops is of utmost importance for the design and development of microfluidic devices[37]. Realizing the importance of droplet manipulation using electric field in microfluidic devices, we have developed a computational method based on three dimensional level set method and the Melcher–Taylor's leaky-dielectric model for two-phase EHD. The developed method is then implemented to sort the droplet in a rectangular microfluidic channel with an orthogonal side branch using dielectrophoresis (DEP). Dielectrophoresis (DEP) is the motion of a droplet in a spatially non-uniform electric field. Recently DEP has been playing a significant role in cell characterization[38] and diagnosis of cancer cells[39].There are two types of DEP motion: positive DEP and negative DEP. If the droplet has lower permittivity than the suspending fluid, it will be attracted to the stronger field regions which is known as positive DEP (pDEP). On the other hand, when the permittivity of the droplet is higher than the suspending fluid, it will be repelled from the electric field which is known as negative DEP (nDEP).

The DEP force for an insulating spherical particle was first analytically defined by Pohl [40]. Motivated by the pioneering work of Pohl [40], Feng[41] first analytically computed the DEP velocity of a leaky dielectric drop in the presence of an axisymmetric nonuniform electric field which is generated by combining uniform and quadruple electric field. In his study Feng[41] concluded that DEP velocity of a drop is governed by the combined influence of EHD and DEP force. Later, Baret et al.[42] developed a Fluorescence Assisted Droplet Sort-

[a)]Electronic mail: nabila.naz@canterbury.ac.uk.
[b)]Electronic mail: y.sui@qmul.ac.uk.

ing (FADS) device by coupling the fluorescence signal with non-uniform electric field. FADS device depends on laser induced fluorescence to detect the chemical contents within a series of droplets which are continuously passing an excitation light spot. In addition to the fluorescence signal, an electronic sorting unit is placed at the downstream of the channel to steer the droplets into the desired branching channel based on their fluorescence signal intensity . Loo et. al[43] developed a high throughput fluorescence-activated droplet sorting of 1 nL droplets using a the sequentially addressable dielectrophoretic array (SADA). Link et. al.[44] reported an electric droplet manipulation platform based on electrophoresis where the droplet is pre-charged and electrochemical reaction occurs between the droplet and the system. Mhatre and Thaokar[45] investigated the DEP motion of perfectly conducting and leaky dielectric drops in a pin-plate electrode assembly. From their study, they have observed that perfectly conducting drop showed pDEP while leaky dielectric drop showed pDEP or nDEP depending on the electrical properties.

However, at present most of the researches on droplet sorting using DEP are based on experimental study. In the experimental study[46], the most common material for fabrication of microfluidic devices is polydimethylsiloxane (PDMS). PDMS is a transparent polymer material which can be molded using standard soft lithography techniques[47,48]. Electric field is incorporated by patterning indium tin oxide (ITO) electrodes on the surface of the glass slide close to the channels. PDMS are strongly hydrophobic and can be directly used to generate water droplet in a suspending oil phase. This facilitates the sorting of droplets and eliminates the cross-contamination caused by surface interactions. The DEP force depends on a number of parameters such as the arrangement of the electrode, electric field distribution, conductivity and permittivity of the droplet with respect to the suspending fluid. However, analysing the effect of these parameters on droplet sorting through experimental investigations are merely difficult, time-consuming, and expensive compared to the numerical analysis. Numerical simulation can analyse the DEP sorting efficiency by changing the relevant parameters in microfluidic environment before performing laboratory experiment. Therefore, computational method can significantly contribute to the design improvement of the microfluidic devices.

Several numerical studies on dielectrophoretic particle-particle interaction and motion have been done using finite element methods (FEM) with an Arbitrary Lagrangian–Eulerian (ALE) algorithm[49,50] in two-dimensions. However, FEM requires very fine mesh when particles are closely spaced or near the electrode which makes them computationally inefficient. In addition to it, a moving mesh is required to update the particle location for ALE algorithm. A finite volume method (FVM) for predicting particle trajectory in dielectrophoretic motion was proposed by Al-Jarro et al.[51]. A coupled immersed interface–boundary-element method ((IIM-BEM)) was developed by Le et.al.[52] for dielectrophoretic particle trapping. They used BEM for computing electric field whereas IIM was used to solve viscous fluid flow problem. However, their developed method is based on two-dimensional geometry and not convenient for large systems. Very recently, Amini and Mohammadi[53] developed a GPU-accelerated immersed boundary–lattice Boltzmann simulation for microparticle separation. Derakhshan et. al.[54] used OpenFOAM for the design and numerical investigation of a circular microchannel for particle/cell separation using dielectrophoresis . There are several other numerical studies which computed the DEP force and particle trajectories in microfluidic channel[55,56] . The main drawback of these studies is that they did not consider the interfacial phenomena. In this research, we have developed a 3d level set method for two-phase EHD problem. The developed method is also implemented to sort the droplet in microfluidic channel using dielectrophoresis.

While cell sorting using an electric field has been the subject of many investigations in the past years, the numerical analysis of droplet sorting has received very little attention. Thus, an accurate fundamental understanding on computational method for DEP assisted droplet sorting either for 2d and 3d geometries is still missing in the literature. This analysis of droplet sorting is of significant importance in the field of microfluidics which involve droplet manipulation using an electric field for biomedical and chemical application. Motivated by this consideration, in the present work we have developed a three dimensional level set method for two-phase electrohydrodynamics. Based on the developed computational method, we have analysed a DEP influenced droplet sorting on microfluidic channel based on several important parameters of the system which can assist the droplet sorting in a microfluidic channel.

The present paper is organized as follows: governing equations, non-dimensional numbers and dynamics of EHD induced droplet deformation are detailed in section II. In section III, we have validated the developed method for a droplet subjected to uniform electric field case. After that, in section III we have applied the present method to analyse the path selection of the droplet depending on different parameters of the system. Finally conclusions on the present numerical method is drawn in section VI.

II. PROBLEM FORMULATION

In this research, a three dimensional level set method is developed for two phase electrohydrodynamics for sorting droplet using non-uniform electric field. At first, the developed method has been validated for a classical fluid flow problem which is droplet subjected to uniform electric field.

A. Problem description

For this problem, we consider an initially uncharged liquid droplet of radius, R suspending in another immiscible fluid. The two fluids have been considered as leaky dielectric having separate fluid and electric properties such as: densities ρ_1 and ρ_2, viscosities μ_1 and μ_2, electric permittivities ε_1 and ε_1 and conductivities K_1 and K_2. The subscripts 1 and 2 refer to

the physical parameters inside and outside of the droplet respectively. We use the suspending fluid as the reference fluid.

A three dimensional (3d) Cartesian co-ordinate is defined with the x axis along the horizontal direction, y axis along the lateral direction and z axis along the vertical direction. Droplet origin is fixed at the center of the computational domain. The top and bottom walls are separated by a distance 2H and subjected to a uniform electric field of strength E_∞ in the transverse direction. The top wall is connected to the positive electrode of electric potential, $\Phi = HE_\infty$ and the bottom wall is connected to the negative electrode of electric potential, $\Phi = -HE_\infty$ as shown in FIG 1. At drop surface the polar angle θ is measured counter clock-wise from negative z-axis. Here, $\theta = 0^\circ, 180^\circ$ are defined as pole region whereas $\theta = 90^\circ$ is defined as equator region.

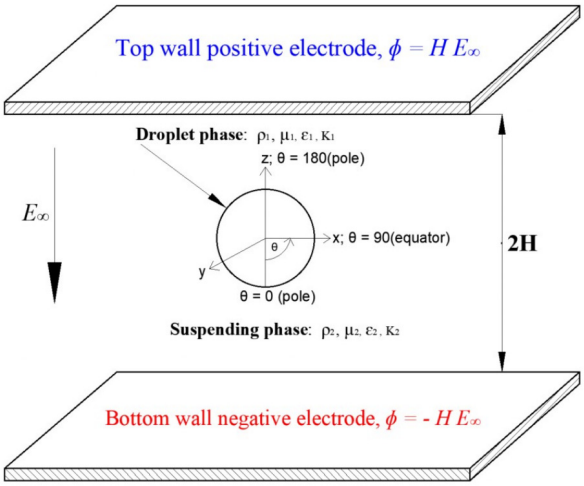

FIG. 1. Schematic illustration of a droplet suspended in another fluid and subjected to a uniform electric field, E_∞

.

B. Governing equations

We have assumed both of the fluids of the system are immiscible and incompressible. Therefore, the continuity Eq. (1) and momentum equation Eq. (2) in the dimensional form are expressed as:

$$\nabla.\vec{u} = 0, \tag{1}$$

$$\rho\left[\frac{\partial \vec{u}}{\partial t} + (\vec{u}.\nabla)\vec{u}\right] = -\nabla p + \nabla.\left[\mu\left(\nabla\vec{u} + \nabla\vec{u}^T\right)\right] + \sigma\kappa\delta_s\vec{n} + \vec{F}_e, \tag{2}$$

where ρ is the fluid density, $\vec{u}$ is the velocity vector, σ is the surface tension coefficient, $\vec{n}$ is the normal to the interface and $\kappa = -\nabla.\mathbf{n}$ is the interface curvature. The surface tension terms only acts on the interface which is represented by the Dirac delta function, δ_s. The effect of electric field is incorporated into the momentum equation by the electrostatic force, $\vec{F}_e$.

1. Determination of electric force, $\vec{F}_e$

The electric field effects are described using electrostatic model. The essential formulation of EHD problems is based on the Maxwell stress tensor which couples the electrostatic and hydrodynamics[57]. Electric force can be written as the divergence of electrostatic Maxwell stress tensor, $\vec{T}_e$:

$$\vec{T}_e = \varepsilon\left(\vec{E}\vec{E} - \frac{E^2}{2}\mathbf{I}\right), \tag{3}$$

by applying the divergence operator:

$$\vec{F}_e = \nabla\cdot\vec{T}_e = q\vec{E} - \frac{1}{2}E^2\nabla\varepsilon. \tag{4}$$

In Eq. (4), first term of the right hand side represents Coulomb forces due to presence of free charges while the second term represents permittivity gradient force due to the difference in permittivity between two phases. Using the $\vec{F}_e$ term, the governing equation for EHD can be written as:

$$\rho\left[\frac{\partial \vec{u}}{\partial t} + (\vec{u}.\nabla)\vec{u}\right] = -\nabla p + \nabla.\left[\mu\left(\nabla\vec{u} + \nabla\vec{u}^T\right)\right] + \sigma\kappa\delta_s\vec{n} + (q\vec{E} - \frac{1}{2}E^2\nabla\varepsilon). \tag{5}$$

The electric field $\vec{E}$ can be defined by the negative gradient of electric potential (Φ) as following:

$$\vec{E} = -\nabla\Phi. \tag{6}$$

Charge conservation equation for the surface charge density q_s can be expressed as[58]:

$$\frac{\partial q_s}{\partial t} + \nabla\cdot(q_s\vec{u}) - \nabla\cdot(K\nabla\Phi) = 0. \tag{7}$$

At the present work, we have considered the deformation behaviour of a leaky dielectric drop in another leaky dielectric fluid under a static electric field. According this model, in spite of having very small electrical conductivity (K), electric charges always accumulate at the fluid interface almost instantly compared with the time scale of the fluid motion. Thus, the equation for the surface charge (q_s) conservation Eq. (7) can be simplified as:

$$\nabla\cdot(K\nabla\Phi) = 0. \tag{8}$$

2. Non-dimensional numbers

We non-dimensionalize the governing equations by using the following characteristic scales[59]: length $\rightarrow R$, velocity(

$u_c) \rightarrow \varepsilon_e {E_\infty}^2 R/\mu_e$, time $\rightarrow R/u_c$, electric field $\rightarrow E_\infty$, viscous stress $\rightarrow \mu_e u_c/R$, electric stress $\rightarrow \varepsilon_e {E_\infty}^2$. The scale of velocity is obtained by equating the order of magnitude of the viscous stress with the electric stress. Based on the above characteristic scales following non-dimensional numbers and the property ratios are obtained:

- *Reynolds number, Re :* measures the ratio of inertial forces to viscous forces.

$$Re = \frac{\rho_2 \varepsilon_2 E_\infty^2 R^2}{\mu_2^2}, \tag{9}$$

where ρ_2, μ_2 are density and viscosity of suspending fluid, R is the droplet radius.

- *Electric Capillary number, Ca_E :* measures the intensity of electric stress over surface tension.

$$Ca_E = \frac{\varepsilon_2 E_\infty^2 R}{\gamma}, \tag{10}$$

where γ is the interfacial tension and E_∞ is the uniform electric field intensity.

- *Electric conductivity ratio, (K)*: It measures the ratio of the conductivity between the droplet (K_1) and suspending fluid (K_2).

$$K = \frac{K_1}{K_2}. \tag{11}$$

- *Electric permittivity ratio, (Q)*: It measures the ratio of the permittivity between the droplet (ε_1) and suspending fluid (ε_2).

$$Q = \frac{\varepsilon_1}{\varepsilon_2}. \tag{12}$$

- *Viscosity ratio, (r_v)*: It measures the ratio of the viscosity between the droplet (μ_1) and suspending fluid (μ_2).

$$r_v = \frac{\mu_1}{\mu_2}. \tag{13}$$

- *Density ratio, (r_d)*: It measures the ratio of the density between the droplet (ρ_1) and suspending fluid (ρ_2).

$$r_d = \frac{\rho_1}{\rho_2}. \tag{14}$$

Based on the dimensionless numbers above, the momentum equation (Eq. 2) can be non-dimensionalized as follow:

$$\rho_c \left[\frac{\partial \vec{u}}{\partial t} + (\vec{u}.\nabla)\vec{u}\right] = -\nabla p + \frac{1}{Re}\nabla.\left[\mu_c\left(\nabla\vec{u} + \nabla\vec{u}^T\right)\right] + \frac{1}{CaRe}\sigma\kappa\delta_s\vec{n} + \frac{Ca_E}{CaRe}\left(q\vec{E} - \frac{1}{2}E^2\nabla\varepsilon\right). \tag{15}$$

C. Dynamics of EHD induced droplet deformation

Based on small perturbation theory, the EHD problem has been solved analytically by Taylor[60] and then by Ajayi[61] to the first and second order in electric capillary number, Ca_E. They characterise the total deformation of a spheroid droplet by means of the parameter D given by the expression:

$$D = \frac{L-B}{L+B}, \tag{16}$$

where L and B are the droplet lengths parallel and perpendicular to the electric field.. Using a linearised asymptotic analysis and assuming that both fluids are extremely viscous and conducting, Taylor[60] also provided an expression for D as a function of the fluid properties and the electric field intensity:

$$D = \frac{9}{16(2K+1)^2}\left[\frac{3K(3r_v+2)(1-KQ)}{5(r_v+1)} + K^2(1-2Q) + 1\right]Ca_E, \tag{17}$$

According to Taylor's model, the droplet can deform into either prolate ($D > 0$) or oblate shape ($D < 0$) depending on the ratio conductivity (K) to the permittivity (Q) of the fluid. The relationship between K and Q is defined by a ratio named α which is the ratio of charge relaxation time scale of suspending fluid, (τ_2^E) to the charge relaxation time scale of drop,(τ_1^E). The charge relaxation time scale, (τ_E) represents the time required by the charges to reach the interface by the sole effect of Ohmic conduction.

$$\alpha = \frac{K}{Q} = \frac{\tau_2^E}{\tau_1^E}, \tag{18}$$

where, $\tau_1^E = \frac{\varepsilon_1}{K_1}$, $\tau_2^E = \frac{\varepsilon_2}{K_2}$.

Different droplet behaviour at different combination of K and Q at $Ca_E << 1$, Re = 0.1, and $r_d = 1$, $r_v = 1$ is illustrated in FIG 2. This figure has been previously presented by several researchers[62–64] for their EHD study. We have reproduced this figure in order to identify the three fluid system that we used in our validation study. In FIG 2, when the values of K and Q fall on the solid curve, the droplet remains spherical which means D = 0. Along the dashed line, $\alpha = 1$. These solid and dashed line divide the parameter space into three regions namely region 1,2 and 3. We have considered three leaky dielectric fluid systems denoted by prolate A (PR_A), prolate B (PR_B) and oblate (OB) which fall into region 1,2, and 3 respectively as shown through three symbols on the FIG 2. For PR_A, $\alpha > 1$ whereas for PR_B and OB $\alpha < 1$.

For $\alpha > 1$: The charge relaxation timescale of the drop fluid is faster than suspending fluid ($\tau_1^E < \tau_2^E$) . Therefore, charges from the drop fluid reaches at the equilibrium state much faster than the suspending fluid. As a result, surface charge distribution is mainly controlled by the charges brought from the drop fluid. In this case, the drop dipole moment takes the same direction as the applied electric field and charges at the poles are attracted toward the electrodes and pull the droplet into a prolate, (PR_A) shape[65,66] as shown as an inset (1) of FIG 2.

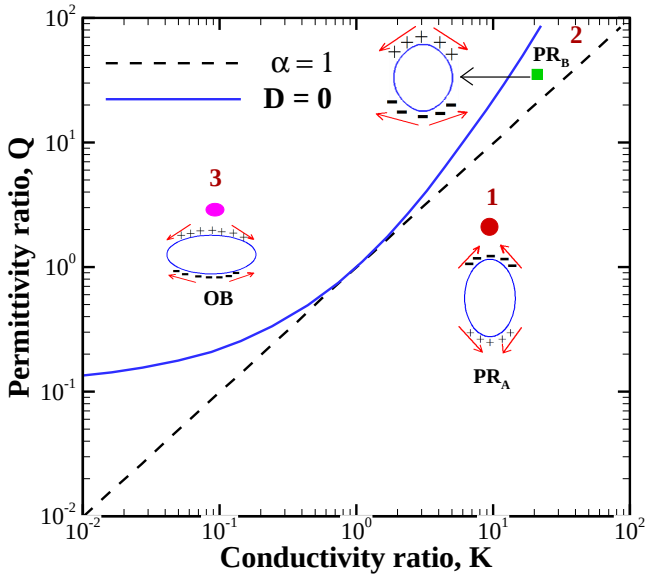

FIG. 2. Different droplet behaviour in the K-Q parameter space reproduced from small deformation theory[62,63]. Here $Ca_E << 1$, Re = 0.1, and $r_d = \rho_1/\rho_2$, $r_v = \mu_1/\mu_2$. The solid line divides the region of prolate (PR) and oblate (OB) drops. The dashed line separates the region of prolate A (PR_A) from prolate B (PR_B) drops. The three symbols on the diagram represent the three systems considered in this study.

For $\alpha < 1$: the charge relaxation timescale of the suspending fluid is faster than the drop fluid ($\tau_1^E > \tau_2^E$). As a result, charges from the suspending fluid reaches at the equilibrium state much faster than the drop fluid. In this case, surface charge distribution is mainly controlled by the charges brought from the suspending fluid. Consequently, the drop dipole moment takes the opposite direction of applied electric field and charges at the poles are repelled from the electrodes and push the droplet into either prolate B or oblate *OB* shape[65,66] as shown as insets (2) and (3) respectively of FIG 2.

III. VALIDATION OF THE METHOD

The computational domain used in the present simulation is a cubic box. Due to the symmetry of the problem, only half of the domain is simulated. Symmetric boundary condition is used at x and y directions for both flow field and the electric potential. While at z direction, no-slip boundary condition is used for the flow field and Dirichlet boundary condition are imposed for the electric potential. The uniform rectangular meshes are used to discretize the computational domain. The validation is performed by comparing the present results with the theoretical, numerical and experimental results of other researchers. For all validation mesh density, dx = 1/64 and computational domain size 4R×4R×24R are used which are sufficient to capture the important characteristics.

1. Prolate droplet deformation

For prolate deformation, , we have modeled two fluid systems denoted by PR_A and PR_B. For PR_A: (K,Q) = (10.0, 1.37) while for PR_B: (K,Q) = (25.0, 50.0). These fluid systems resemble a real fluid system consisting of silicone oil droplet suspended in castor oil which are also used by several researchers[63,67] in their experimental and numerical study. Both silicone and castor oil are weakly conductive fluid and have comparable densities but have difference in viscosity. Due to the high viscosity of the suspending castor oil, the silicone drop falls slowly which makes it easier to observe its behaviour. Therefore, the physical properties of the silicone oil drop in castor oil are ideal for modelling a realistic leaky dielectric drop in a leaky dielectric fluid system.

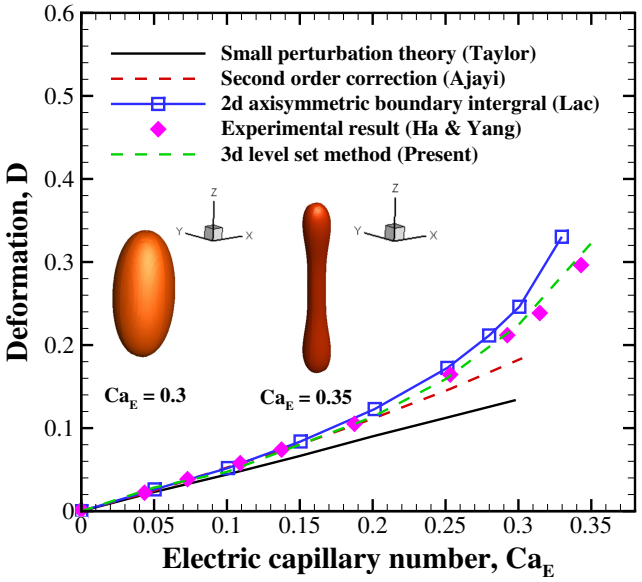

FIG. 3. Droplet deformation as a function of electric capillary number, Ca_E, for prolate droplet at K =10.0, Q =1.37, Re = 0.1, and $r_d = 1$, $r_v = 0.874$. Inset showing 3d droplet deformation for prolate A droplet at $Ca_E = 0.3$ and $Ca_E = 0.35$.

When the electric field is applied, the electrical stresses are generated across the drop and suspending fluid interface, which not only leads to deformation of the droplet but also generates an electrohydrodynamic induced flow in and around the droplet. The droplet deformation is mainly governed by electric capillary number, Ca_E which is the ratio of electric stress to surface tension. With the increase of Ca_E, the intensity of electric stress increases over the surface tension which leads to larger EHD induced droplet deformation.

The quantitative comparisons of Taylor deformation as function of Ca_E for PR_A fluid is shown in FIG 3. This figure shows that the droplet deforms into a prolate shape and the magnitude of deformation increase with the increasing value of Ca_E. When Ca_E is increased from 0.3 to 0.35, the electric stress is sufficiently strong to overcome the surface tension which leads to a sudden elongation and break-up of the droplet as shown inset of FIG 3. Here, the deformation pa-

rameter obtained from present simulation is validated by the existing analytic, numerical and experimental results. For analytical comparison, the present results are compared to the first- and second-order theory of Taylor[60] and Ajayi[61]. Analytical comparison clearly depicts that the deformation curve obtained from present simulation quickly deviates from the first-order theoretical prediction of Taylor[60]. However, the present results show good agreement with second order corrections of Ajayi[61] up to $Ca_E = 0.2$. A reasonable agreement is also obtained among the present results and the axisymmetric boundary integral solution of Lac and Homsy[63] and also with the experimental data provided by Ha and Yang[67].

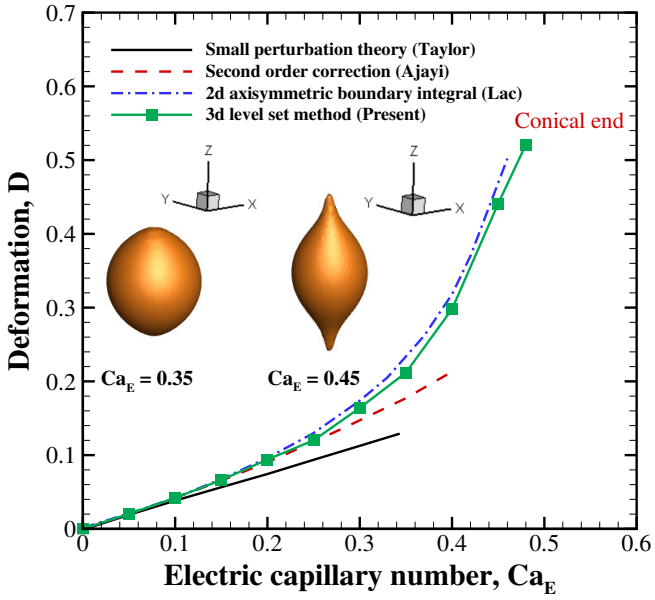

FIG. 4. Droplet deformation as a function of electric capillary number, Ca_E, for prolate droplet at K =25.0, Q =50.0, Re = 0.1, and $r_d = 1$, $r_v = 0.874$. Inset showing 3d droplet deformation for prolate B droplet at $Ca_E = 0.35$ and $Ca_E = 0.45$.

The quantitative comparisons of Taylor deformation as function of Ca_E for PR_B fluid is shown in FIG 4. Here, the deformation parameter obtained from present simulation is validated by the existing analytic, and numerical results. This figure shows that the droplet deforms and forms conical ends at both ends. With the increasing value of Ca_E, the conical ends become more prominent and form Taylor cones. When two Taylor cone develop at its opposing ends, infinitely long thin liquid charged jets start to form from these ends which is known as EHD tip streaming. Inset of FIG 4 shows the onset of tip streaming at $Ca_E = 0.45$.

For analytical comparison, the present results are compared to the first- and second-order theory of Taylor[60] and Ajayi[61]. Analytical comparison clearly depicts that the deformation curve obtained from present simulation quickly deviates from the first-order theoretical prediction of Taylor[60]. However, the present results show good agreement with second order corrections of Ajayi[61] up to $Ca_E = 0.25$. A good agreement is also obtained between the present results and the axisymmetric boundary integral solution of Lac and Homsy[63].

2. *Oblate droplet deformation*

For oblate deformation, we have modeled a fluid system denoted by *OB* with (K,Q) = (0.10, 2.0). This fluid system is also used by Lac and Homsy[63] in their axisymmetrical study of EHD induced droplet deformation.

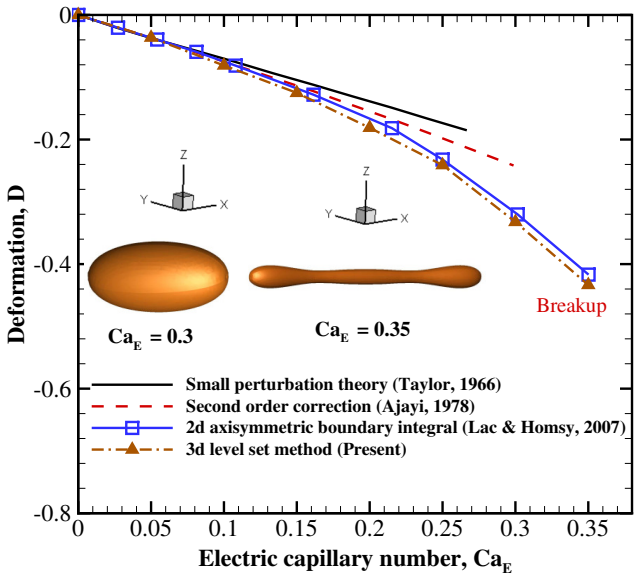

FIG. 5. Droplet deformation as a function of electric capillary number, Ca_E, for oblate droplet at K =0.10, Q =2.0, Re = 0.1, and $r_d = 1$, $r_v = 0.874$. Inset showing 3d droplet deformation for oblate droplet at $Ca_E = 0.3$ and $Ca_E = 0.35$.

Similar to prolate droplet, the deformation of oblate droplet is also controlled by electric capillary number Ca_E. The effect of different electric capillary number (Ca_E) on droplet deformation for *OB* system fluid is shown quantitatively in FIG 5. From the fig, it is depicted that the droplet deformation increases with the increase of Ca_E and maximum deformation occurs at the perpendicular direction of applied field which leads to oblate shape droplet. Here, the droplet reaches the steady shape upto Ca_E = 0.3. After that at Ca_E = 0.35, the droplet no longer takes steady shape and with time it elongates more and more and form bulbous shape at two ends which can lead to breakup as shown inset of FIG 5.

The deformation parameter obtained from present simulation for *OB* fluid system is validated by the existing first and second order perturbation theory of Taylor[60] and Ajayi[61] as shown in FIG 5. Results obtained from the present simulation deviates from the analytical results after $Ca_E = 0.1$ as analytical results fails to capture larger deformation. However, the present result show a good agreement with the axisymmetric boundary integral solution of Lac and Homsy[63] as shown in FIG 5.

IV. APPLICATION OF THE METHOD

A. Sorting of droplet using non-uniform electric field

DEP is the motion of a droplet in a spatially non-uniform electric field .When an initially uncharged drop suspending in another fluid is subjected to a spatially non-uniform electric field, all the free charges from both fluids get accumulated at the interface and the particle get polarized. Due to non-uniformity of the electric field, charges at the interface generate non-equal Columbic forces which causes the DEP motion of the droplet in a particular direction depending on the electrical properties.

For an insulating spherical particle of radius R, in a nonuniform electric field E, the net DEP force is first defined by Pohl [40].

$$\mathbf{F}_{\mathrm{DEP}} = 2\pi R^3 \varepsilon_0 \varepsilon_{\mathrm{m}} \beta \nabla \mathbf{E}^2, \tag{19}$$

where R is the droplet radius, ε_{m} is the permittivity of the fluid, $\varepsilon_0 = 8.854 \times 10^{-12}$ F/m is the vacuum permittivity and $\mathbf{E}$ is the electric field intensity. $\beta(\omega)$ is the real part of the frequency-dependent Clausius–Mossotti factor which is given by:

$$\beta(\omega) = \mathrm{Re}\left(\frac{\varepsilon_{\mathrm{p}}^* - \varepsilon_m^*}{\varepsilon_{\mathrm{p}}^* + 2\varepsilon_{\mathrm{m}}^*}\right), \tag{20}$$

$\varepsilon_{\mathrm{p}}^*$ and $\varepsilon_{\mathrm{m}}^*$ are the complex permittivity of the drop and the fluid, respectively.

There are two types of DEP motion: positive DEP and negative DEP. If the droplet has lower permittivity than the suspending fluid, it will be attracted to the stronger field regions which is known as positive DEP (pDEP). On the other hand, when the permittivity of the droplet is higher than the suspending fluid, it will be repelled from the electric field which is known as negative DEP (nDEP) .

B. Problem statement

We consider an initially uncharged liquid droplet of radius R suspending in another medium flowing through a rectangular channel with an orthogonal side branch as shown in FIG 6 (a). Both the straight channel and the side branch have the constant cross section $4l^2$ with a side length of $2l$. The length of the parent channel is $8l$ whereas the length of the two daughter channels are $6l$. Here, the considered length is long enough for the droplet to reach a steady shape before reaching the bifurcation region. The fluid motion is governed by the incompressible Navier–Stokes equations. No-slip boundary condition is imposed at the channel wall. Fully developed laminar channel flow profiles are set at the inlet and two outlets with flow rates Q_0, Q_1, Q_2 respectively in a way that $Q_0 = Q_1 + Q_2$. The droplet is initially placed along the centreline of the parent channel at a distance of $2l$ from the inlet which helps to get the steady state after travelling a distance of 6l. A three-dimensional Cartesian coordinate system is used with x-axis along the axis of the main channel, z-axis along the side branch axis and the origin of the coordinate system is located at the intersection of the two centre lines of two daughter channels. The droplet and suspending medium are considered as water and oil having different physical and electric properties such as: densities ρ_1 and ρ_2, viscosities μ_1 and μ_2, electric permittivities ε_1 and ε_1 and conductivities K_1 and K_2. The subscripts 1 and 2 refer to the physical parameters inside and outside of the droplet respectively. We use the suspending fluid as the reference fluid.

If a spatially non-uniform electric field is generated inside a microchannel which is containing a droplet, the droplet faces DEP motion and moves in a particular direction. In practical DEP applications, the non-uniform can be generated in two ways. One way is to use electrodes of different shapes, size and designs [68] and another way is changing the position of the electrode at different position of the microfluidic channel.

In this research work, we have generated the non-uniform electric field inside the microfluidic channel by placing a rectangular electrode at the bottom of the channel with specific voltage. When a voltage is applied along a device, the electric field creates a linear gradient which allows the droplet to experience a spatial difference in electric field within the channel. We have considered two electrode positions at a distance of 4l and 6l from the inlet as shown in FIG 6 (b) and (c) respectively. The electrode positions are referred as electrode position 1 and electrode position 2. Length, width and height of both electrodes are 4l, 2l and l respectively where l is the half length of the cross-sectional width. With the presence of these electrode positions, electric field intensity is defined by capillary number Ca_E.

1. Non-dimensional numbers

The problem depends on a number of dimensionless parameters based on the flow configuration, hydrodynamic and electric properties of the drop and suspending fluid.

- *Branch flow ratio, (q)* measures the flow rate ratio of branch channel to main channel.

$$q = \frac{Q_2}{Q_1 + Q_2}, \tag{21}$$

  where Q_1 and Q_2 are the flow rates in the downstream main channel and in the side channel, respectively, as indicated in FIG 6

- *Reynolds number, (Re)* measures the ratio of inertial forces to viscous forces.

$$Re = \frac{\rho_2 u l}{\mu_2}, \tag{22}$$

  where u is the mean velocity of the Poiseuille flow imposed at the inlet of the main channel and l is the half-cross-sectional dimension of the main channel.

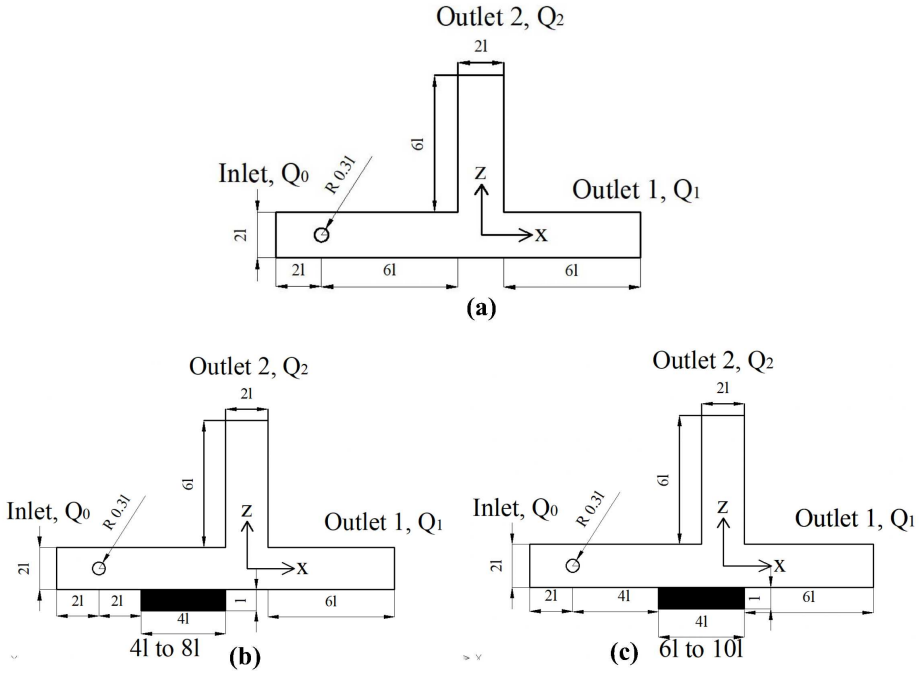

FIG. 6. Geometry of the rectangular channel with an orthogonal side branch: (a) without electrode; (b) electrode at position 1; (b) electrode at position 2.

.

- *Electric conductivity ratio, (K)*: It measures the ratio of the conductivity between the droplet (K_1) and suspending fluid (K_2)as defined in Eq. 11.

- *Electric permittivity ratio, (S)*: It measures the ratio of the permittivity between the droplet (ε_1) and suspending fluid (ε_2) as defined in Eq. 12.

- *Viscosity ratio, (r_v)*: It measures the ratio of the viscosity between the droplet (μ_1) and suspending fluid (μ_2) as defined in Eq. 13.

- *Density ratio, (r_d)*: It measures the ratio of the density between the droplet (ρ_1) and suspending fluid (ρ_2) as defined in Eq. 14.

- *Hydrodynamic Capillary number, Ca :* measures the intensity of viscous stress over surface tension.

$$Ca = \frac{\mu_2 u}{\gamma}, \tag{23}$$

- *Electric Capillary number, (Ca_E)* measures the intensity of electric stress over surface tension.

$$Ca_E = \frac{\varepsilon_2 E^2 l}{\gamma}, \tag{24}$$

where γ is the interfacial tension, l is the half-cross-sectional dimension of the main channel. and E is the electric field intensity.

- *Size ratio, (λ)*: It measures the ratio of the droplet radius (R) to the half-cross-sectional dimension of the main channel (l).

$$\lambda = \frac{R}{l}. \tag{25}$$

V. PATH SELECTION OF THE DROPLET

In this problem, we have considered leaky dielectric-leaky dielectric fluid system consisting of water droplet suspending in soybean oil. This fluid system is also used in experimental study of Ahn et.al.[16]. The physical properties considered in this research are: K = 0.107, S = 1.34, r_d = 1.09, r_v = 0.018, $\lambda = 0.2, 0.3, 0.4$, Ca = 0.1, Ca_E = 0, 0.4, 0.9, Re = 1, 20 and different branch flow ratios q = 0.1 - 0.7. When this system of fluid is subjected to non-uniform electric field it shows negative DEP motion as permittivity ratio >1 (S>1), which means that the permittivity of the droplet is higher than the permittivity of the suspending fluid. Therefore the droplet will be repelled from the electric field.

At first, we investigate the influence of mesh size on the trajectories of the droplet in x-z plane for three mesh densities which are dx = dy = dz = 1/16, 1/32 and 1/64 . FIG 7 shows the influence of different mesh resolution on the trajectories the droplet flowing in the main channel for Re = 20.0, Ca = 0.1, $Ca_E = 0$, q = 0.3 $\lambda = 0.3$, r_d = 1.09, and r_v = 0.018 . It is obtained that the trajectories for dx = 1/32 and 1/64 are almost superimposed on each other. Therefore, we chose dx = 1/32

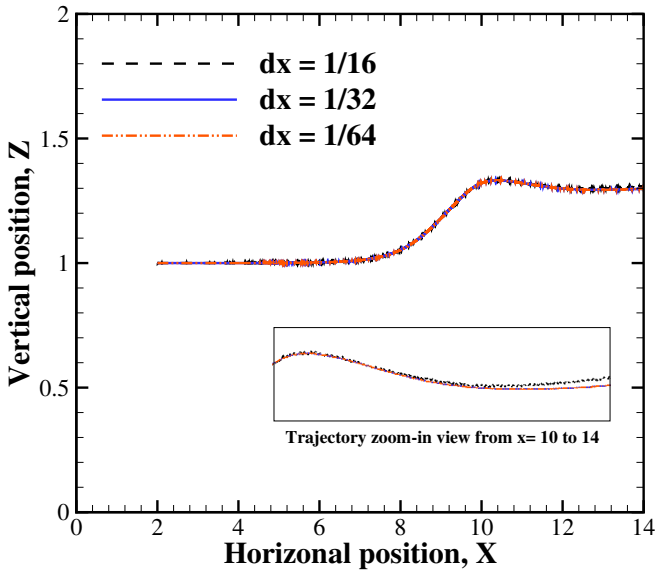

FIG. 7. Trajectories of a droplet (R/L = 0.3) flowing in the main channel at Re = 20.0, Ca = 0.1, $Ca_E = 0$, q = 0.3, r_d = 1.09, and r_v = 0.018 with three different mesh sizes

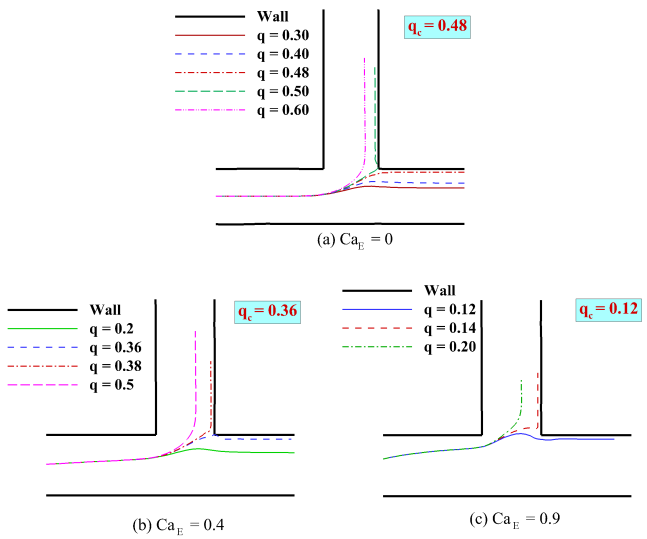

FIG. 8. Effect of electric field strength, (Ca_E) on the droplet trajectory at different branch flow ratio, (q). Other parameters, Re = 1.0; Ca = 0.1, $\lambda = 0.3$, $r_d = 1.09$, and $r_v = 0.018$

for the current simulation having around 20 meshes across the diameter of the droplet which is sufficient enough to capture the important characteristics and mass of the droplet can also be conserved reasonably well with the relative mass change within 0.3%.

The main objective of this research work is to characterize the path selection of the droplet as a function of different physical parameters. A simple way to characterize sorting of a droplet is to define the critical branch ratio, q_c, above which the droplet enters the side branch. Thus the droplet flows into the main channel after the bifurcation region if $q \leq q_c$ otherwise, it flows into the side branch. In the following section, we have investigated the effect of electric capillary number (Ca_E), electrode positions, inertia (Re) and size ratio (λ) on the path selection of the droplet. For each case at a fixed value of particular physical properties, we progressively increase q from 0.1 by large steps of $\Delta q = 0.1$ until we find the transition, where the droplet flows into the side branch rather than the main channel. Around the transition region, we then refine the step to $\Delta q = 0.02$.

A. Effect of electric field, (Ca_E) at Re = 1

In this section, we have analysed the effect of electric field on the path selection of the droplet at a rectangular microchannel. The electric field effect is incorporated inside the channel by placing an electrode at the bottom of the channel with a specific voltage. We have considered 2 and 3V electric potential which corresponds to electric capillary number, Ca_E = 0.4 and 0.9 respectively.

FIG 8 shows the mass trajectories of the droplet's centre of

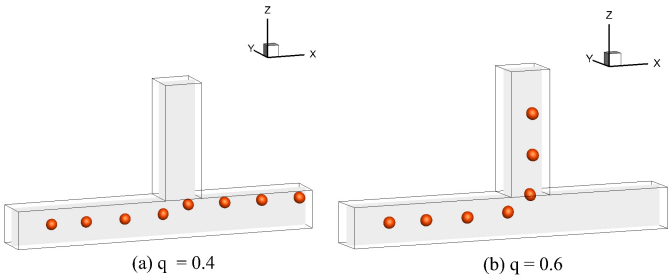

FIG. 9. The difference in path selection of the droplet at without electric field ($Ca_E = 0$) for branch flow ratio q = 0.4 and 0.6. Other parameters, Re = 1.0; Ca = 0.1, $\lambda = 0.3$, $r_d = 1.09$, and $r_v = 0.018$

mass for Ca_E = 0, 0.4, and 0.9. Ca_E is defined as the ratio of electric stress over surface tension. At Ca_E = 0, the electric field is absent and the path selection of the droplet depends on only branch flow ratio, q and Reynolds number, Re.

FIG 8 (a) shows the mass centre trajectory of the droplet at Ca_E = 0 and Re = 1 for different branch flow ratios. From the mass centre trajectory it is depicted that without electric field, the droplet moves along the centre line of the main channel before the bifurcation region. When the droplet comes to the bifurcation region, it first attracted by the orthogonal side branch. If the value of $q > 0.48$, the droplet enters to the side branch otherwise, it moves back towards the main channel after passing the bifurcation region. Therefore the critical branch flow ratio without electric field is $q_c = 0.48$ at Re = 1.

The time evolution of the droplet profiles without electric field ($Ca_E = 0$) at Re = 1 are shown in FIG 9 for (a) q = 0.4 and (b) q = 0.6 respectively. From the figure it is obtained that at $Ca_E = 0$, the droplet takes the branch which receives the

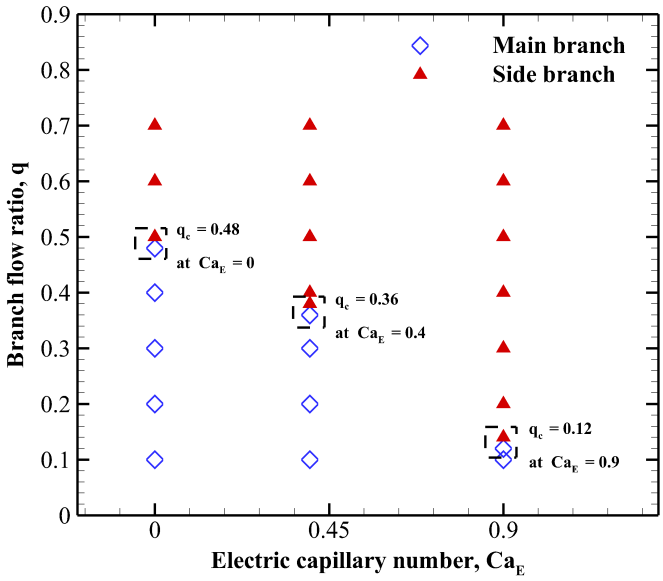

FIG. 10. Branch flow ratio as a function of electric capillary number. Other parameters, Re = 1.0; Ca = 0.1, electrode position 1, $\lambda = 0.3$, $r_d = 1.09$, and $r_v = 0.018$.

higher flow rate. Consequently it follows into the downstream main channel towards outlet 1 at q = 0.4 where the flow rate of the outlet 2 is lower than the outlet 1. When the flow rate of outlet 2 is increased to 0.6, the droplet enters to the side branch which can be sorted from outlet 2.

On the application of electric field with Ca_E = 0.4 and 0.9, it is obtained that the droplet enters the side branch even at lower branch flow ratio. At Ca_E = 0.4, the droplet enters the side branch from q = 0.38 whereas at Ca_E = 0.9, it enters the side branch at very low value of branch flow ratio which is q = 0.14. Therefore, electric field plays a significant role in reducing the value of critical branch flow ratio q_c.

A phase diagram for branch flow ratio (q) as a function of electric capillary number (Ca_E) is shown in FIG 10 for a droplet flowing in a microchannel without electric field and with electric field through an electrode at position 1. Without electric field, it is obtained that the q_c = 0.48 for Re = 1. When a non-uniform electric field is introduced through an electrode at distance of 4l from the inlet (position 1), the obtained q_c = 0.36 and 0.12 for Ca_E = 0.4 and 0.9 respectively. Therefore, electric field can play a significant role in reduction of q_c which can faciliates the sorting of the droplet at desired outlet.

The time evolution of droplet profile at q = 0.2 are shown in FIG 11 for Ca_E = 0.4, and 0.9 respectively. In this research we have considered water droplet suspending in soybean oil. For this system, permittivity of the droplet is higher than the suspending fluid which gives rise to negative dielectrophoresis (nDEP) motion. Due to nDEP, the droplet starts to repel from the centre of the channel when it comes close to the electrode. Larger the value of Ca_E, larger the repulsive force acts on the droplet which promotes the sorting of the droplet at the side branch even at smaller value of q. Therefore at q = 0.2, the

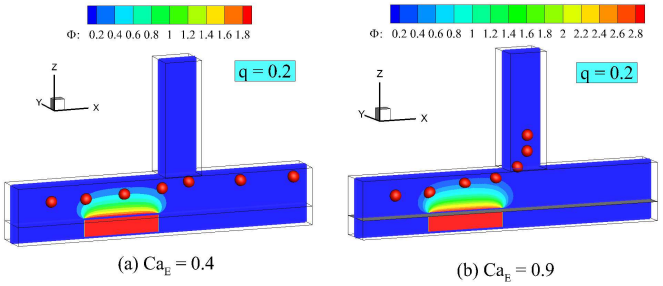

FIG. 11. The difference in path selection of the droplet at (a) $Ca_E = 0.4$ and (a) $Ca_E = 0.9$ for same branch flow ratio q = 0.2 and electrode position 1 . Other parameters, Re = 1.0; Ca = 0.1, $\lambda = 0.3$, $r_d = 1.09$, and $r_v = 0.018$

droplet favours the side branch at Ca_E = 0.9 while it flows into the downstream main channel at Ca_E = 0.4.

B. Effect of electrode position at Re = 1

We have considered two electrode positions at a distance of 4l and 6l from the inlet as shown in FIG 6 (b) and (c) respectively. Length, width and height of both electrodes are 4l, 2l and 1 respectively where 1 is the half length of the cross-sectional width.

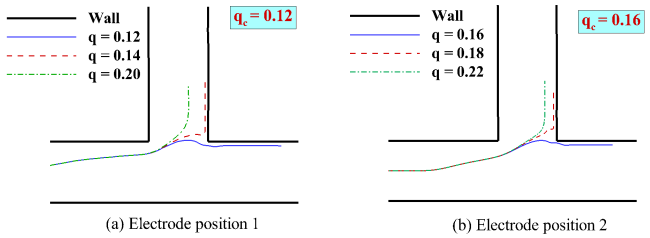

FIG. 12. Effect of electrode position on the droplet trajectory at different branch flow ratio, (q). Other parameters, Re = 1.0; Ca = 0.1, $Ca_E = 0.9$, $\lambda = 0.3$, $r_d = 1.09$, and $r_v = 0.018$

FIG 12 present the effect of electrode position on the droplet trajectory at different branch flow ratio, (q). From the mass centre trajectory it is depicted that for both electrode positions, the droplet move along the centre line of the main channel until it comes closer to the electrode position which is 4l and 6l position from the inlet for electrode position 1 and 2 respectively. Here both electrodes create a spatially non-uniform electric field with electric potential of 3 volt which corresponds to $Ca_E = 0.9$. When the droplet comes closer to the electrode, it deforms in an oblate shape as conductivity ratio is less than the permittivity ratio, (K<S). In addition to it, the droplet also faces the repulsive electric force due to negative DEP (nDEP) and move far away from the centreline and reaches the bifurcation region. At the bifurcation region, it slows down and first attracted by the orthogonal side branch.

For electrode position 1, this electric repulsive electric force overcome the hydrodynamic force and the droplet enters into the side branch when $q > 0.12$ otherwise, it moves back towards the main channel after passing the bifurcation region as shown in FIG 12(a). However when we move the electrode from position 1 to 2, it is found that the value of q at which the droplet enters the side branch increases. For electrode position 2, the droplet enters into the side branch if $q > 0.16$. Therefore, the closer the electrode to the droplet initial position, the lower the critical branch flow ratio for sorting is obtained.

C. Effect of inertia, Re

We now investigate the trajectory of the droplet for higher Reynolds number at different branch flow ratios, q. FIG 13 presents the trajectories of the droplet's centre of mass for Re = 1 and 20 at different branch flow ratios. Here, other parameters are: Ca = 0.1, $Ca_E = 0.0$, $\lambda = 0.3$, $r_d = 1.09$, and $r_v = 0.018$. The figure illustrates that the mass centre trajectory of the droplet for Re = 20 follows the same pattern as Re = 1. The droplet remains the centerline of the channel before reaching the bifurcation region. When the bifurcation region starts, the droplet first attracted towards the side branch. After passing the bifurcation region at Re = 1, the droplet enters into the side branch at and above equal branch flow ratio (q = 0.5). Therefore without electric field ($Ca_E = 0.$) the critical branch flow ratio, q_c = 0.48 at Re = 1. However, when then the inertia effect is increased to Re = 20, the value of q_c is also increased to 0.62.

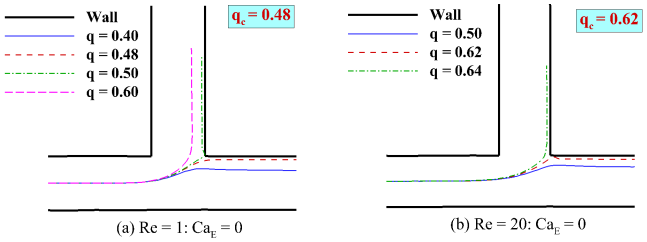

FIG. 13. Effect of inertia on the droplet trajectory at different branch flow ratios, (q). Other parameters, Ca = 0.1, $Ca_E = 0.0$, $\lambda = 0.3$, $r_d = 1.09$, and $r_v = 0.018$

The time evolution of the droplet profiles without electric field ($Ca_E = 0$) at q = 0.5 are shown in FIG 14 for (a) Re = 1 and (b) Re = 20 respectively. From the figure it is obtained that at equal branch flow ratio, the droplet selects the path towards the orthogonal side branch at Re = 1 whereas it goes back to the main channel when inertia effect is increased to Re = 20.

Therefore it is found that when the flow is governed only by poiseuille flow, the inertia plays an important role on critical branch flow ratio (q_c) above which sorting can be achieved. In most practical application, sorting will be delayed where inertia effect is significant. Here it comes the necessity of droplet manipulation for rapid sorting. In the following section, we will study how non-uniform electric field can facilitate the droplet sorting even at higher Re.

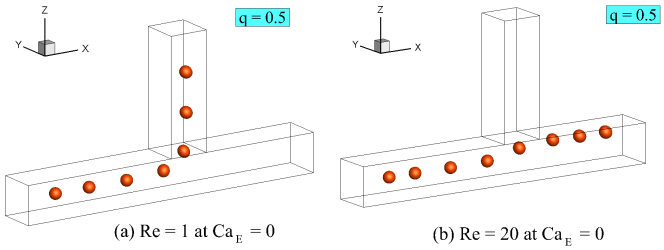

FIG. 14. The difference in path selection of the droplet at (a) Re = 1 and (b) Re = 20 at same branch flow ratio, q = 0.5. (q). Other parameters, Ca = 0.1, $Ca_E = 0.0$, $\lambda = 0.3$, $r_d = 1.09$, and $r_v = 0.018$

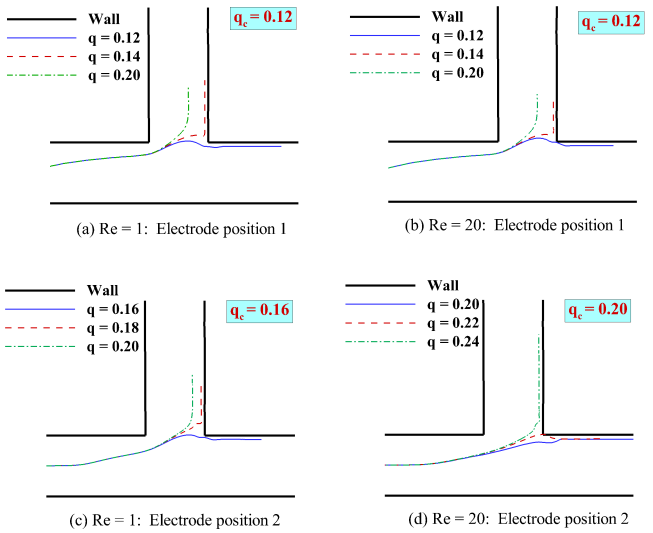

FIG. 15. Combined effect of inertia and electrode positions on the droplet trajectory at different branch flow ratios, (q). Other parameters, Ca = 0.1, $Ca_E = 0.9$, $\lambda = 0.3$, $r_d = 1.09$, and $r_v = 0.018$

FIG 15 shows the combined effect of inertia (Re = 1 and 20) and electric field ($Ca_E = 0.9$) on the droplet trajectory at different branch flow ratios (q) with electrode positions 1 (a,b) and electrode positions 2 (c,d). From the figure it is obtained that when the electrode is at position 1, the droplet takes the side branch when q> 0.12 both for Re =1 and 20. However at electrode position 2, the droplet takes the side branch at q> 0.16 and q> 0.22 for Re =1 and 20 respectively. Therefore for electrode position 1, critical branch ratio q_c = 0.12 both for Re = 1 and 20. On the other hand, for electrode position 2, q_c = 0.16 at Re = 1 and q_c = 0.22 at Re = 20. For both electrode positions, the presence of electric field promotes the droplet sorting at lower branch flow ratio (q) even at higher inertia regime which can not be obtained without electric field effect. Moreover at electrode position 1, we get the same value of q_c for both lower and higher inertia effect. Therefore, in practical

application where inertia is significant, placing an electrode closer to the droplet with sufficient electric potential can speed up the sorting process with a lower value of q_c.

D. Effect of size ratio, λ at Re = 20

In this section we have investigated the effect of droplet size ratio ($\lambda = R/l$), with Re = 20, electrode at position 1 and $Ca_E = 0.9$. We have considered three different size ratios, λ = 0.2,0.3, and 0.4. The trajectories of the droplet's centre of mass and a phase diagram for different branch flow ratios are shown in FIG 16 and FIG 17 for different branch flow ratios at λ = 0.2,0.3, and 0.4. From the figures, it is observed that at a given value of other parameters, the size ratio, λ has significant effect on the path selection of the droplet. At λ = 0.2, after passing the bifurcation region the droplet follows the path towards the straight channel upto q = 0.28 after that it enters into the side branch. Therefore, the critical branch ratio, q_c = 0.28 at λ = 0.2. When the increase the size ratio to λ = 0.3, q_c is reduced to 0.12. Further increase of size ratio to λ = 0.4 leads to further reduction of q_c which is 0.08. This reduction of the value of q_c as a function of λ is also illustrated in FIG 17 through a phase diagram. As dielectrophoresis force is proportional to the droplet radius, larger droplet undergoes higher dielectrophoresis force which promotes the droplet sorting at the side branch even at the lower value of branch flow ratio.

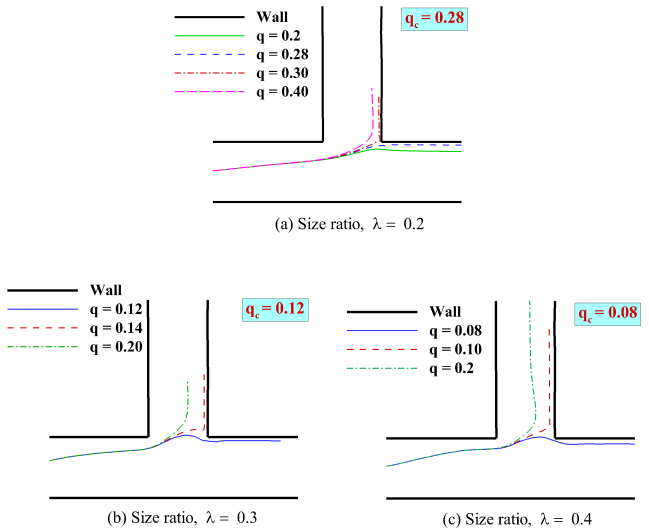

FIG. 16. Effect of droplet size on the droplet trajectory at different branch flow ratio, (q). Other parameters, Re = 20.0; Ca = 0.1, Ca_E = 0.9, electrode position 1, $r_d = 1.09$, and $r_v = 0.018$

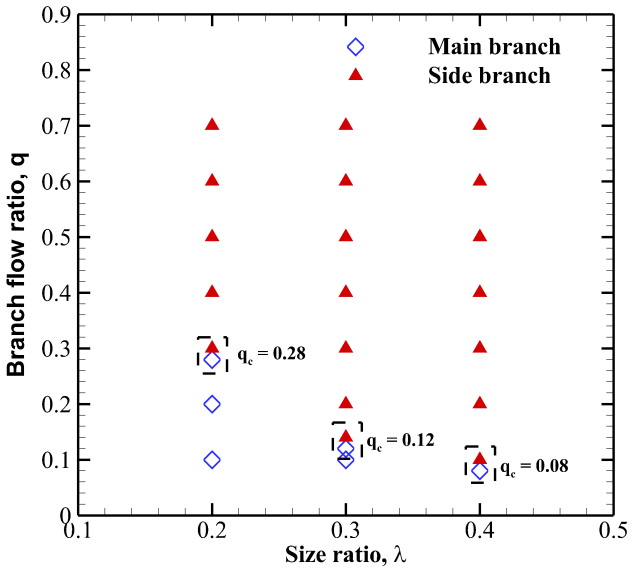

FIG. 17. Branch flow ratio as a function of size ratio. Other parameters, Re = 20.0; Ca = 0.1, $Ca_E = 0.9$, electrode position 1, $r_d = 1.09$, and $r_v = 0.018$.

VI. CONCLUSIONS

In this research work, we have developed a 3d dimensional level set model for two-phase EHD problem. The developed model has been implemented to a practical engineering problem of droplet sorting in microfluidics. In this study, we consider a water droplet suspending in soybean oil and flowing through a rectangular channel with an orthogonal side branch. Main findings from the present analysis are summarized as follows:

i) Three types of droplet deformation namely prolate A (PR_A), prolate B(PR_B), and oblate (OB) drop is obtained depending on the ratio of K and Q which is defined by $\alpha = K/Q$. If $\alpha > 1$, the droplet takes PR_A shape. However when $\alpha < 1$, the droplet can take either PR_B or OB shape.

ii) The results obtained from the present simulation show good agreement with the existing analytical result of Taylor[60] and Ajayi[61], axisymmetric boundary integral solution of Lac and Homsy[63] and experimental results provided by Ha and Yang[67].

iii) Without any electric field effect (Ca_E = 0), the droplet trajectory is mainly governed by the value of q and Re. At low value of inertia, the droplet favours the outlet which receives higher flow rate. However when inertia effect is significant, the droplet takes the outlet 1 even it receives lower flow rate until q_c is achieved.

From the present analysis we find that without electric field effect, q_c for droplet sorting are 0.48 and 0.62 for Re = 1 and 20 respectively which implies that the inertia has a leading role on increasing the value of q_c.

iv) The spatially non-uniform electric field is created by placing a single electrode at the bottom of the microchannel. Electric field intensity is represented by electric capillary number, (Ca_E). We have investigated trajectory of the droplet for different branch flow ratios (q) for two different values of Ca_E which are 0.4 and 0.9 and compared it to the result without electric field effect ($Ca_E = 0$) . It has been observed that higher the value of Ca_E, higher the reduction of critical branch flow ratio (q_c) is observed.

At $Ca_E = 0$, the critical branch flow ratio is q_c = 0.48 at low inertia (Re = 1). However, at Ca_E =0.4 and 0.9, the branch flow ratio reduces to q_c = 0.36 and 0.12 at the same inertia (Re = 1). Therefore, spatially non-uniform electric field can play a significant role in droplet sorting at desired outlet.

v) Next, we study the effect of electrode positions on the path selection of the droplet. Two electrode positions are considered namely electrode 1 and electrode 2 which are placed at a distance of 4l and 6l from the inlet of the channel. At electrode position 1, q_c = 0.12 at Re = 1. When electrode is move to position 2, a slight increase of critical branch ratio is obtained which is q_c = 0.16 at the same Re. Therefore the closer the electrode is placed from the initial position of the droplet, smaller the critical branch flow ratio.

vi) After that, we studied the effect on inertia by increasing the value of Re from 1 to 20. When there is no electric field effect (Ca_E = 0.0), it has been obtained that the value of q_c = 0.62 at Re = 20 whereas it is 0.48 at Re = 1. Therefore, without any electric field at high Re, the droplet can flow into the downstream main channel even when it receives lesser flow rate than the side branch.

However when electric field is applied at higher inertia, it is still possible to sort the droplet at side branch at lower value of q_c. For example at electrode position 1, we have obtained q_c = 0.12 both for Re = 1 and 20. For electrode position 2, q_c is increased from 0.16 to 0.22 when Re is increased from 1 to 20 which is still lower than the value of q_c without electric field at high inertia . Therefore with electric field, the droplet can be manipulated to sort at the side branch even at a higher inertia with smaller value of q_c.

vii) Finally we analyse the effect of size ratio (λ) on the path selection of the selection when electrode is placed at position 1 with Ca_E = 0.9 and Re =20. We consider three different value of λ which are 0.2, 0.3 and 0.4. It is obtain that with the increase of the value of λ, a reduction of the value of q_c is obtained. When we increase the value of λ from 0.2 to 0.3, we obtain the reduction of q_c = 0.28 to 0.12. After that when we further increase the value of λ to 0.4, a very small value of q_c is obtained which is 0.08. Larger the size ratio (λ), the larger the value of dielectrophoresis force acting on the droplet which promotes the droplet sorting at side branch even at lower branch flow ratio with high inertia effect.

viii) To conclude, from the present investigation we have observed that electrode at position 1 with Ca_E = 0.9 and λ = 0.4, the critical branch flow ratio is the lowest q_c which is 0.08.

VII. SCOPE OF FUTURE STUDY

In the present work we developed a three-dimensional level set method for two-phase electrohydrodynamics (EHD) problem which opens a myriad of scope for future studies. Authors primary focus is to study the path selection of the droplet without and with electric field effect as a function of different parameters of the system. Based on the observation of the present work, a simplified model can be developed which can help understand the droplet sorting mechanism when subject to non-uniform electric field. The authors study the dielectrophoresis assisted droplet sorting for rectangular microchannel with cartesian grids. Therefore, the present model can be improved to deal with complex geometry for example, microchannel with Y-bifurcation. Additionally, further parametric analysis can be performed to elucidate the effect of other parameters such as multiple number of droplets and electrodes, complex interactions between the droplet themselves, or more interestingly different geometry of the microchannel including a series of successive bifurcations.

ACKNOWLEDGMENTS

We wish to acknowledge the Queen Mary PhD Research Studentship and High Performance Computing (HPC) facilities of Queen Mary University of London, UK. N.Naz is grateful to Dr. Shubhadeep Mandal, Dr Ahmed Ismail and Dr. Kang Luo for insightful discussions on droplet EHD.

DATA AVAILABILITY

The data that support the findings of this study are available from the corresponding author upon reasonable request.

Appendix A: Numerical Procedures

In this research we have developed a three dimensional level set method for two phase electrohydrodynamics. The non-dimensional partial differential equations are discretised using the finite volume method on a staggered grid with velocity and electric field components are defined at the cell faces and scalar variables (e.g. pressure, electric properties and the level-set function) at the cell centres as shown in FIG 18.

The motion of the interface is dependent on the evolution of the velocity field, therefore the advection of the level-set function and the Navier-Stokes equations must be solved in a manner that is temporally matched. In our numerical simulation, the following computational order is followed from time level n to n + 1:

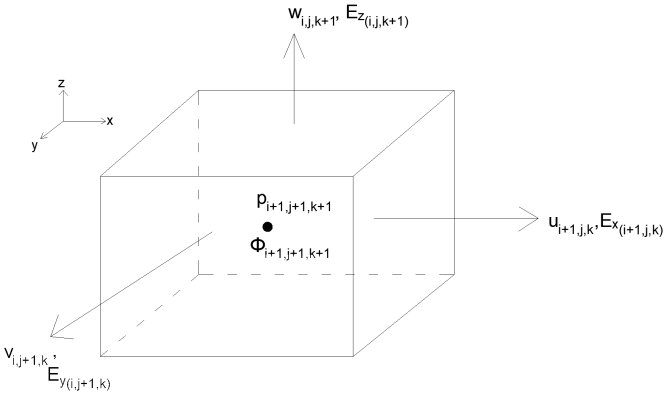

FIG. 18. Position of variables in a three-dimensional mesh cell.

1. Update the level-set function through the advection equation using the velocity field at time level n and n - 1 using Eq. (A1).

2. Determine the surface tension force at the time level n + 1/2 using the averaged value of the level-set function at time level n and n + 1 using Eq. (A2).

3. Determine the electric potential at the time level n + 1/2 using Eq. (A3).

4. The electric field is then straightforwardly computed at the time level n + 1/2 by taking the negative gradient of electric potential at the same time level using Eq. (A4).

5. Determine the electric charge at the time level n + 1/2 using Eq. (A5).

6. Determine the electric force term at the time level n + 1/2 using the value of electric field and electric permittivity at the same time level using Eq. (A6).

7. Update the velocity field for time level n + 1 by solving the momentum and continuity equations with Eq. (A9).

1. Updating the level-set function to determine the surface tension force

The update the level-set function at time level n and n - 1 is done through the following advection equation:

$$\phi^{n+1} = \phi^n - \Delta t \left\{ 1.5\mathscr{W}\left[(\mathbf{u}\cdot\nabla\phi)^n\right] - 0.5\mathscr{W}\left[(\mathbf{u}\cdot\nabla\phi)^{n-1}\right]\right\}. \tag{A1}$$

The Crank-Nicholson method is used for the discretisation of the time-stepping procedure and the Adams-Bashforth method for the advective term. $\mathscr{W}$ is the discrete convection operator where fifth-order weighted essentially non-oscillatory (WENO) scheme is applied. The 'reinitialisation' step is applied after solving the advection equation to make sure that ϕ^{n+1} is kept approximately the signed distance function. Once ϕ^{n+1} is updated, the intermediate value of $\phi^{n+\frac{1}{2}}$ is used to calculate the physical properties of the fluids at the interface and the surface tension forces.

$$\phi^{n+\frac{1}{2}} = \frac{\phi^n + \phi^{n+1}}{2}. \tag{A2}$$

a. Determining the electric force

For leaky-dielectric fluids, the electric potential, Φ at the time level n + 1/2 is determined by solving the following equation by successive over-relaxation (SOR) iterative method. SOR method shows a good performance in terms of number of iteration and computational time.

$$\nabla\cdot\left(K_{n+\frac{1}{2}}\nabla\Phi_{n+\frac{1}{2}}\right) = 0. \tag{A3}$$

Electric field, $\vec{E}_{n+\frac{1}{2}}$ is then determined from following:

$$\vec{E}_{n+\frac{1}{2}} = -\nabla\Phi_{n+\frac{1}{2}}. \tag{A4}$$

The electric charge, q at the time level n + 1/2 is determined by solving the following equation:

$$\nabla\cdot(\varepsilon_{n+\frac{1}{2}}\nabla\Phi_{n+\frac{1}{2}}) = -(q)_{n+\frac{1}{2}}. \tag{A5}$$

Finally, the electric force, $\vec{F}_{e_{n+\frac{1}{2}}}$ then obtained from following:

$$\vec{F}_{e_{n+\frac{1}{2}}} = \nabla\cdot(\varepsilon_{n+\frac{1}{2}}\nabla\Phi_{n+\frac{1}{2}})\vec{E}_{n+\frac{1}{2}} - \frac{1}{2}E^2\nabla\varepsilon_{n+\frac{1}{2}}. \tag{A6}$$

2. Solving the momentum and continuity equations

The projection method[69] provides an efficient way to solve for velocity and pressure field by coupling the momentum equation and the continuity equation. First, the pressure term is removed from the momentum equation and an intermediate velocity $\vec{u}_*$ is obtained through a semi-implicit discretisation and is solved by successive over-relaxation (SOR) iterative method.

$$\rho_{n+\frac{1}{2}}\left[\frac{\vec{u}_* - \vec{u}_n}{\Delta t}\right] = -\left[\frac{3}{2}\mathscr{H}(\vec{u}_n) - \frac{1}{2}\mathscr{H}(\vec{u}_{n-1})\right] +$$

$$\frac{1}{2Re}\left[\mathscr{L}(\vec{u}_n, \mu_{n+1/2}) + \mathscr{L}(\vec{u}_*, \mu_{n+1/2})\right] +$$

$$\frac{1}{Ca_E Re}\sigma\kappa\delta(n+\frac{1}{2})\vec{n} + \frac{1}{Re}\vec{F}_{e_{n+\frac{1}{2}}} \tag{A7}$$

where $\mathscr{H}$ represents the discrete convection operator and $\mathscr{L}$ denotes the discrete diffusion operator.

In order to obtain a divergence-free velocity field, the intermediate velocity $\vec{u}_*$ is corrected by:

$$\frac{\vec{u}_{n+\frac{1}{2}} - \vec{u}_*}{\Delta t} = -\frac{\nabla p_{n+\frac{1}{2}}}{\rho_{n+\frac{1}{2}}} \tag{A8}$$

Since the velocity field at time level n + 1 is divergence free, we first calculate the pressure field by solving the pressure Poisson equation using the SOR method.

$$\frac{\nabla p_{n+\frac{1}{2}}}{\rho_{n+\frac{1}{2}}} = -\frac{\nabla \cdot \vec{u}_*}{\Delta t} \tag{A9}$$

Once the pressure field is obtained, the velocity field at time level n + 1 is calculated with Eq. A9.

[1] O. A. Basaran, H. Gao, and P. P. Bhat, "Nonstandard inkjets," Annual Review of Fluid Mechanics **45**, 85–113 (2013).

[2] Z.-M. Huang, Y.-Z. Zhang, M. Kotaki, and S. Ramakrishna, "A review on polymer nanofibers by electrospinning and their applications in nanocomposites," Composites science and technology **63**, 2223–2253 (2003).

[3] J. Shrimpton and A. Yule, "Characterisation of charged hydrocarbon sprays for application in combustion systems," Experiments in fluids **26**, 460–469 (1999).

[4] J. B. Fenn, M. Mann, C. K. Meng, S. F. Wong, and C. M. Whitehouse, "Electrospray ionization for mass spectrometry of large biomolecules," Science **246**, 64–71 (1989).

[5] N. A. Brown, J. N. Gladstone, and P. R. Chiarot, "Materials printing using electrospray," in *ASME 2014 International Mechanical Engineering Congress and Exposition* (American Society of Mechanical Engineers, 2014) pp. V02BT02A049–V02BT02A049.

[6] M. Windbergs, Y. Zhao, J. Heyman, and D. A. Weitz, "Biodegradable core–shell carriers for simultaneous encapsulation of synergistic actives," Journal of the American Chemical Society **135**, 7933–7937 (2013).

[7] S. S. Datta, A. Abbaspourrad, E. Amstad, J. Fan, S.-H. Kim, M. Romanowsky, H. C. Shum, B. Sun, A. S. Utada, M. Windbergs, *et al.*, "25th anniversary article: Double emulsion templated solid microcapsules: Mechanics and controlled release," Advanced Materials **26**, 2205–2218 (2014).

[8] Y. Zhang, Y.-P. Ho, Y.-L. Chiu, H. F. Chan, B. Chlebina, T. Schuhmann, L. You, and K. W. Leong, "A programmable microenvironment for cellular studies via microfluidics-generated double emulsions," Biomaterials **34**, 4564–4572 (2013).

[9] C. B. Chang, J. N. Wilking, S.-H. Kim, H. C. Shum, and D. A. Weitz, "Monodisperse emulsion drop microenvironments for bacterial biofilm growth," Small **11**, 3954–3961 (2015).

[10] T. H. Niepa, L. Hou, H. Jiang, M. Goulian, H. Koo, K. J. Stebe, and D. Lee, "Microbial nanoculture as an artificial microniche," Scientific reports **6**, 1–10 (2016).

[11] M. Sivaramakrishnan, R. Kothandan, D. K. Govindarajan, Y. Meganathan, and K. Kandaswamy, "Active microfluidic systems for cell sorting and separation," Current Opinion in Biomedical Engineering **13**, 60–68 (2020).

[12] M. Jacquemond, N. Jeckelmann, L. Ouali, and O. P. Haefliger, "Perfume-containing polyurea microcapsules with undetectable levels of free isocyanates," Journal of applied polymer science **114**, 3074–3080 (2009).

[13] T. Feczkó, V. Kokol, and B. Voncina, "Preparation and characterization of ethylcellulose-based microcapsules for sustaining release of a model fragrance," Macromolecular research **18**, 636–640 (2010).

[14] G. Muschiolik, "Multiple emulsions for food use," Current Opinion in Colloid & Interface Science **12**, 213–220 (2007).

[15] J. J. Agresti, E. Antipov, A. R. Abate, K. Ahn, A. C. Rowat, J.-C. Baret, M. Marquez, A. M. Klibanov, A. D. Griffiths, and D. A. Weitz, "Ultrahigh-throughput screening in drop-based microfluidics for directed evolution," Proceedings of the National Academy of Sciences **107**, 4004–4009 (2010).

[16] K. Ahn, C. Kerbage, T. P. Hunt, R. Westervelt, D. R. Link, and D. A. Weitz, "Dielectrophoretic manipulation of drops for high-speed microfluidic sorting devices," Applied Physics Letters **88**, 024104 (2006).

[17] E. Brouzes, T. Kruse, R. Kimmerling, and H. H. Strey, "Rapid and continuous magnetic separation in droplet microfluidic devices," Lab on a Chip **15**, 908–919 (2015).

[18] A. Ali-Cherif, S. Begolo, S. Descroix, J.-L. Viovy, and L. Malaquin, "Programmable magnetic tweezers and droplet microfluidic device for high-throughput nanoliter multi-step assays," Angewandte Chemie **124**, 10923–10927 (2012).

[19] J. Park, J. H. Jung, K. Park, G. Destgeer, H. Ahmed, R. Ahmad, and H. J. Sung, "On-demand acoustic droplet splitting and steering in a disposable microfluidic chip," Lab on a Chip **18**, 422–432 (2018).

[20] S. Li, X. Ding, F. Guo, Y. Chen, M. I. Lapsley, S.-C. S. Lin, L. Wang, J. P. McCoy, C. E. Cameron, and T. J. Huang, "An on-chip, multichannel droplet sorter using standing surface acoustic waves," Analytical chemistry **85**, 5468–5474 (2013).

[21] S. Cheng and S. Chandra, "A pneumatic droplet-on-demand generator," Experiments in fluids **34**, 755–762 (2003).

[22] C. Huang, W. Fang, M. Ke, H. Chou, and J. Yang, "A biocompatible open-surface droplet manipulation platform for detection of multi-nucleotide polymorphism," Lab on a Chip **14**, 2057–2062 (2014).

[23] N. G. Green, H. Morgan, and J. J. Milner, "Manipulation and trapping of sub-micron bioparticles using dielectrophoresis," Journal of Biochemical and Biophysical Methods **35**, 89–102 (1997).

[24] T. Schnelle, T. Müller, and G. Fuhr, "Trapping in ac octode field cages," Journal of Electrostatics **50**, 17–29 (2000).

[25] J. Voldman, M. Toner, M. Gray, and M. Schmidt, "Design and analysis of extruded quadrupolar dielectrophoretic traps," Journal of electrostatics **57**, 69–90 (2003).

[26] Y. Kang, D. Li, S. A. Kalams, and J. E. Eid, "Dc-dielectrophoretic separation of biological cells by size," Biomedical microdevices **10**, 243–249 (2008).

[27] J. E. Gordon, Z. Gagnon, and H.-C. Chang, "Dielectrophoretic discrimination of bovine red blood cell starvation age by buffer selection and membrane cross-linking," Biomicrofluidics **1**, 044102 (2007).

[28] J. Park, B. Kim, S. K. Choi, S. Hong, S. H. Lee, and K.-I. Lee, "An efficient cell separation system using 3d-asymmetric microelectrodes," Lab on a Chip **5**, 1264–1270 (2005).

[29] J. Kadaksham, P. Singh, and N. Aubry, "Dielectrophoresis induced clustering regimes of viable yeast cells," Electrophoresis **26**, 3738–3744 (2005).

[30] G. H. Markx, Y. Huang, X.-F. Zhou, and R. Pethig, "Dielectrophoretic characterization and separation of micro-organisms," Microbiology **140**, 585–591 (1994).

[31] G. O. Parikesit, A. P. Markesteijn, O. M. Piciu, A. Bossche, J. Westerweel, I. T. Young, and Y. Garini, "Size-dependent trajectories of dna macromolecules due to insulative dielectrophoresis in submicrometer-deep fluidic channels," Biomicrofluidics **2**, 024103 (2008).

[32] F. Grom, J. Kentsch, T. Müller, T. Schnelle, and M. Stelzle, "Accumulation and trapping of hepatitis a virus particles by electrohydrodynamic flow and dielectrophoresis," Electrophoresis **27**, 1386–1393 (2006).

[33] A. Docoslis, L. A. Tercero Espinoza, B. Zhang, L.-L. Cheng, B. A. Israel, P. Alexandridis, and N. L. Abbott, "Using nonuniform electric fields to accelerate the transport of viruses to surfaces from media of physiological ionic strength," Langmuir **23**, 3840–3848 (2007).

[34] B. H. Lapizco-Encinas, B. A. Simmons, E. B. Cummings, and Y. Fintschenko, "Insulator-based dielectrophoresis for the selective concentration and separation of live bacteria in water," Electrophoresis **25**, 1695–1704 (2004).

[35] H. Song, V. Mulukutla, C. D. James, and D. J. Bennett, "Continuous-mode dielectrophoretic gating for highly efficient separation of analytes in surface micromachined microfluidic devices," Journal of Micromechanics and Microengineering **18**, 125013 (2008).

[36] L. Yang, P. P. Banada, A. K. Bhunia, and R. Bashir, "Effects of dielectrophoresis on growth, viability and immuno-reactivity of listeria monocytogenes," Journal of biological engineering **2**, 1–14 (2008).

[37] P. R. Chiarot, P. Sullivan, and R. B. Mrad, "An overview of electrospray applications in mems and microfluidic systems," Journal of Microelectromechanical Systems **20**, 1241–1249 (2011).

[38] E. A. Henslee, "Dielectrophoresis in cell characterization," Electrophoresis **41**, 1915–1930 (2020).

[39] G. I. Russo, N. Musso, A. Romano, G. Caruso, S. Petralia, L. Lanzanò, G. Broggi, and M. Camarda, "The role of dielectrophoresis for cancer di-

agnosis and prognosis," Cancers **14**, 198 (2021).
[40]H. A. Pohl, "Dielectrophoresis," The behavior of neutral matter in nonuniform electric fields (1978).
[41]J. Q. Feng, "Dielectrophoresis of a deformable fluid particle in a nonuniform electric field," Physical Review E **54**, 4438 (1996).
[42]J.-C. Baret, O. J. Miller, V. Taly, M. Ryckelynck, A. El-Harrak, L. Frenz, C. Rick, M. L. Samuels, J. B. Hutchison, J. J. Agresti, *et al.*, "Fluorescence-activated droplet sorting (fads): efficient microfluidic cell sorting based on enzymatic activity," Lab on a Chip **9**, 1850–1858 (2009).
[43]M. H. Loo, Y. Nakagawa, S. H. Kim, A. Isozaki, and K. Goda, "High-throughput sorting of nanoliter droplets enabled by a sequentially addressable dielectrophoretic array," Electrophoresis **43**, 477–486 (2022).
[44]D. R. Link, E. Grasland-Mongrain, A. Duri, F. Sarrazin, Z. Cheng, G. Cristobal, M. Marquez, and D. A. Weitz, "Electric control of droplets in microfluidic devices," Angewandte Chemie International Edition **45**, 2556–2560 (2006).
[45]S. Mhatre and R. M. Thaokar, "Drop motion, deformation, and cyclic motion in a non-uniform electric field in the viscous limit," Physics of Fluids **25**, 072105 (2013).
[46]J. C. McDonald, D. C. Duffy, J. R. Anderson, D. T. Chiu, H. Wu, O. J. Schueller, and G. M. Whitesides, "Fabrication of microfluidic systems in poly (dimethylsiloxane)," ELECTROPHORESIS: An International Journal **21**, 27–40 (2000).
[47]D. C. Duffy, J. C. McDonald, O. J. Schueller, and G. M. Whitesides, "Rapid prototyping of microfluidic systems in poly (dimethylsiloxane)," Analytical chemistry **70**, 4974–4984 (1998).
[48]M. A. Unger, H.-P. Chou, T. Thorsen, A. Scherer, and S. R. Quake, "Monolithic microfabricated valves and pumps by multilayer soft lithography," science **288**, 113–116 (2000).
[49]Y. Ai and S. Qian, "Dc dielectrophoretic particle–particle interactions and their relative motions," Journal of colloid and interface science **346**, 448–454 (2010).
[50]Y. Liu, W. K. Liu, T. Belytschko, N. Patankar, A. C. To, A. Kopacz, and J.-H. Chung, "Immersed electrokinetic finite element method," International Journal for Numerical Methods in Engineering **71**, 379–405 (2007).
[51]A. Al-Jarro, J. Paul, D. Thomas, J. Crowe, N. Sawyer, F. Rose, and K. Shakesheff, "Direct calculation of maxwell stress tensor for accurate trajectory prediction during dep for 2d and 3d structures," Journal of Physics D: Applied Physics **40**, 71 (2006).
[52]D. V. Le, C. Rosales, B. C. Khoo, and J. Peraire, "Numerical design of electrical-mechanical traps," Lab on a Chip **8**, 755–763 (2008).
[53]H. S. Amini and A. Mohammadi, "Microparticle separation using dielectrophoresis-assisted inertial microfluidics: A gpu-accelerated immersed boundary–lattice boltzmann simulation," Physical Review E **107**, 035307 (2023).
[54]R. Derakhshan, A. Ghasemi, R. Moradi, and A. Ramiar, "Design and numerical investigation of a circular microchannel for particle/cell separation using dielectrophoresis," Advanced Powder Technology **34**, 104046 (2023).
[55]N. G. Green, A. Ramos, and H. Morgan, "Numerical solution of the dielectrophoretic and travelling wave forces for interdigitated electrode arrays using the finite element method," Journal of Electrostatics **56**, 235–254 (2002).
[56]H. Li and R. Bashir, "On the design and optimization of micro-fluidic dielectrophoretic devices: a dynamic simulation study," Biomedical microdevices **6**, 289–295 (2004).
[57]J. Hua, L. K. Lim, and C.-H. Wang, "Numerical simulation of deformation/motion of a drop suspended in viscous liquids under influence of steady electric fields," Physics of Fluids **20**, 113302 (2008).
[58]J. López-Herrera, S. Popinet, and M. Herrada, "A charge-conservative approach for simulating electrohydrodynamic two-phase flows using volume-of-fluid," Journal of Computational Physics **230**, 1939–1955 (2011).
[59]M. A. Halim and A. Esmaeeli, "Computational studies on the transient electrohydrodynamics of a liquid drop," Fluid Dyn. Mater. Process **9**, 435–460 (2013).
[60]G. I. Taylor, "Studies in electrohydrodynamics. i. the circulation produced in a drop by an electric field," Proceedings of the Royal Society of London. Series A. Mathematical and Physical Sciences **291**, 159–166 (1966).
[61]O. Ajayi, "A note on taylor's electrohydrodynamic theory," Proceedings of the Royal Society of London. A. Mathematical and Physical Sciences **364**, 499–507 (1978).
[62]S. Torza, R. Cox, and S. Mason, "Electrohydrodynamic deformation and bursts of liquid drops," Philosophical Transactions of the Royal Society of London. Series A, Mathematical and Physical Sciences **269**, 295–319 (1971).
[63]E. Lac and G. Homsy, "Axisymmetric deformation and stability of a viscous drop in a steady electric field," Journal of Fluid Mechanics **590**, 239–264 (2007).
[64]J. C. Baygents, N. Rivette, and H. A. Stone, "Electrohydrodynamic deformation and interaction of drop pairs," Journal of Fluid Mechanics **368**, 359–375 (1998).
[65]J. Melcher, "Electrohydrodynamics: a review of the role of interfacial shear stresses," Ann. Rev. Fluid Mech. **1**, 111–146 (1969).
[66]P. F. Salipante and P. M. Vlahovska, "Electrohydrodynamics of drops in strong uniform dc electric fields," Physics of Fluids **22**, 112110 (2010).
[67]J.-W. Ha and S.-M. Yang, "Deformation and breakup of newtonian and non-newtonian conducting drops in an electric field," Journal of Fluid Mechanics **405**, 131–156 (2000).
[68]L. M. Barrett, A. J. Skulan, A. K. Singh, E. B. Cummings, and G. J. Fiechtner, "Dielectrophoretic manipulation of particles and cells using insulating ridges in faceted prism microchannels," Analytical chemistry **77**, 6798–6804 (2005).
[69]E. G. Puckett, A. S. Almgren, J. B. Bell, D. L. Marcus, and W. J. Rider, "A high-order projection method for tracking fluid interfaces in variable density incompressible flows," Journal of computational physics **130**, 269–282 (1997).